JOURNAL OF CHEMICAL INFORMATION AND MODELING

ARTICLE

pubs.acs.org/jcim

Molecular Modeling and Molecular Dynamics Simulation Studies of the GSK3β/ATP/Substrate Complex: Understanding the Unique P+4 Primed Phosphorylation Specificity for GSK3β Substrates

Shao-Yong Lu,[‡] Yong-Jun Jiang,[*,§] Jian-Wei Zou,[§] and Tian-Xing Wu[‡]

[‡]Department of Chemistry, Zhejiang University, Hangzhou, Zhejiang 310027, China

[§]Key Laboratory for Molecular Design and Nutrition Engineering, Ningbo Institute of Technology, Zhejiang University, Ningbo 315104, China

ABSTRACT: Substrate specificity of protein kinases is of fundamental importance for the integrity and fidelity of signaling pathways. Glycogen synthase kinase 3β (GSK3β) has a unique substrate specificity that prefers phosphorylation of its substrates at the P+4 serine before it can further phosphorylate the substrate at the P0 serine in the canonical motif SXXXS-(p), where S(p) is the primed phosphorylation site. The detailed phosphorylation mechanism, however, is not clearly understood. In this study, a three-dimensional (3D) model of the ternary complex of GSK3β, ATP, and the phosphorylated glycogen synthase (pGS), termed GSK3β/ATP/pGS, is constructed using a hierarchical approach and by integrating molecular modeling and molecular dynamics (MD) simulations. Based on the 3D model, the substrate primed phosphorylation mechanism is investigated via two 12 ns comparative MD simulations of the GSK3β/ATP/pGS and GSK3β/ATP/GS systems, which differ in the phosphate group bound to the P+4 serine of GS. In agreement with structural analysis, computed binding free energies reveal that the binding of pGS to GSK3β is favored in the prephosphorylated state compared with the GS native state. More importantly, comparison with the system simulated without primed phosphorylation in the GSK3β/ATP/GS complex shows that for an optimal phosphorylation reaction to occur, the pGS priming phosphate in the GSK3β/ATP/pGS system optimizes the proper orientation of the GSK3β N- and C-terminal domains and clamps the P0 serine of pGS in the appropriate configuration for interaction with the ATP γ-phosphate within the catalytic groove.

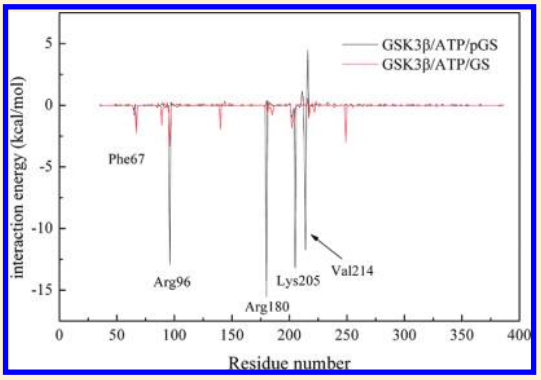

INTRODUCTION

Protein phosphorylation, modulated by protein kinases, is a well-established regulatory mechanism in many cellular processes, including metabolism, growth, division, and differentiation.[1,2] It is initiated by the transfer of γ-phosphate of ATP to the hydroxyl oxygen of the Ser, Thr, and Tyr residues of a kinase-specific protein substrate. There are ~10,000 different target proteins in a typical eukaryotic cell, harboring ~700,000 potential phosphorylation sites (P-sites) for any given kinase.[3] Therefore, the critical aspect of control of cellular processes is the ability of a given protein kinase to discriminate, select, and subsequently phosphorylate only target proteins at specific, functionally relevant amino acid residues.

Kinetic and structural studies have revealed that the structure of the catalytic site of kinases and the difference in charge and hydrophobicity of their surface residues play a pivotal role in substrate specificity. For example, in cyclin-dependent kinase 2 (CDK2), the canonical motif of the substrates is (S/T)PX(K/R), where S/T is the P-site and X is any amino acid. CDK2 has a great specificity for a Pro in the P+1 site of the substrates due to the unique hydrogen-bonding properties of proline-containing peptides. On the other hand, CDK2 prefers a basic residue in the P+3 position of the substrates to interact with the phosphate-Thr160 (p-Thr160) in the kinase.[4] The consensus sequence in substrates recognized by protein kinase A (PKA) is RRX-(S/T)Φ, where Φ is a hydrophobic residue. The basic residues at the P-3 and P-2 positions of the substrates interact with the two negatively charged Glu127 and Glu230 of PKA. In addition, Φ at the P+1 site fits into a hydrophobic pocket in PKA, which is lined by Leu198 and Leu205.[5] However, unlike many other protein kinases, glycogen synthase kinase 3 (GSK3) has a unique specificity for its substrates. It prefers phosphorylation of its substrates at the P+4 site before it can further phosphorylate the substrate at the P0 site in the canonical motif SXXXS(p), where S(p) is the primed phosphorylation site.

GSK3 was discovered in the early 1980s,[6] and since then great progress has been made in characterizing this multifunctional kinase. The best known role of GSK3 is in insulin signaling and metabolic regulation; there is also evidence that links GSK3 activity to the regulation of embryogenesis, inflammation, and neuroplasticity.[7,8] Recent investigations have revealed that GSK3 is involved in cellular pathways and pathologies of several diseases, such as type 2 diabetes, cancer, Alzheimer's disease, chronic inflammation, and bipolar disorder.[9,10] Mammalian cells

Received: December 12, 2010
Published: April 16, 2011

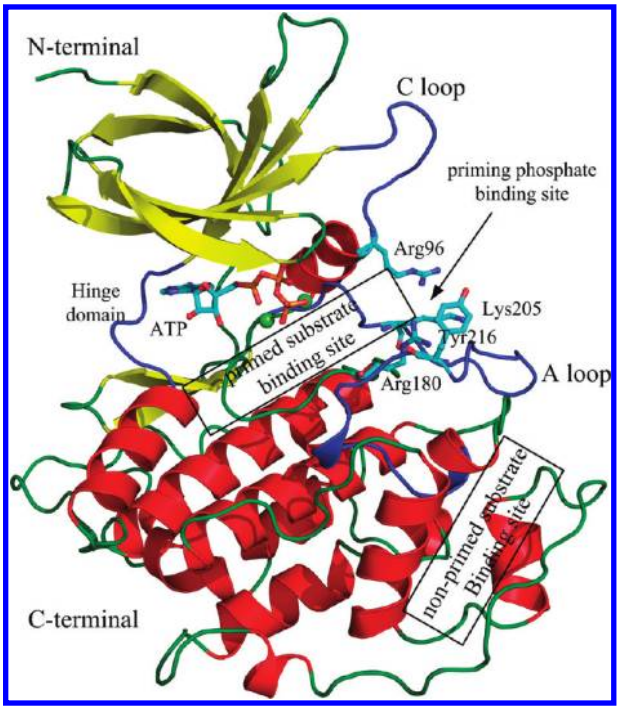

Figure 1. The secondary structure of the GSK3β-AMP complex (PDB code 1PYX). The small N-lobe (35−132) and large C-lobe (139−383) are marked. The β-sheet, α-helix, and loop are colored yellow, red, and green, respectively, with the C loop (89−95), hinge domain (133−138), and A loop (200−226) in blue. ATP is represented in sticks, and the two green spheres represent the two Mg^{2+} ions present in the active site. The A loop runs along the surface of the primed substrate binding groove. The nonprimed substrate binding site is located at the kinase's C-terminal helical domain. The Arg96, Arg180, and Lys205 positive triad constitutes the priming phosphate binding site. The phenol side chain of unphosphorylated Tyr216 is protruding into the primed substrate groove.

have two GSK isoforms, namely, α and β. Here, the enzymatic function of GSK3β, the most physiologically, biochemically, and structurally characterized kinase of the GSK3 family, is examined.

Figure 1 shows the structure of GSK3β, highlighting the active site and important domains which govern substrate binding. The crystallographic structure of GSK3β is mostly similar to that of P38γ,[11] a member of the mitogen-activated protein kinases. Structural alignment of P38γ and GSK3β reveals that the phosphate-Thr183 (p-Thr183) interacts with the arginine residues Arg73, Arg152, and Arg176, which correspond to Arg96, Arg180, and Lys205 of GSK3β. The Arg96/Arg180/Lys205 basic triad constitutes the priming phosphate binding site of GSK3β substrates. Mutation of the triad prevents phosphorylation of GSK3β substrates.[12,13] The GSK3β residue that is equivalent to Thr183 of P38γ, however, is the nonphosphorylatable residue Asn213. This indicates the requirement of a prephosphorylated residue of the substrates to play the role of p-Thr183 in the alignment of the N- and C-terminal domains of the kinase. In protein kinases P38γ,[11] CDK2,[4] and PKA,[5] the phosphothreonine residues (p-Thr183 for P38γ, p-Thr160 for CDK2, and p-Thr197 for PKA) at the activation loop (A loop), which serve as a phosphorylation-sensitive switch for substrate binding, appear to induce the active conformation of this loop for optimal catalytic activity. In contrast, the superimpositions of GSK3β X-ray structures with and without a phosphate ion in the priming phosphate binding site show that the A loops in both structures have similar active conformations.[14] This indicates that the active conformation of GSK3β is not induced by phosphorylation when the priming phosphate of the substrate binds to GSK3β. The in-depth mechanism, however, is poorly understood.

In insulin signal transduction, the N-terminus Ser9 of GSK3β is phosphorylated by protein kinase B. The phosphoserine, acting as a pseudosubstrate, occupies the same binding site as the priming phosphate of the substrate and blocks access to the catalytic site. Subsequently, the phosphorylation and inactivation of GS by GSK3β are completely prevented; this contributes to the stimulation of glycogen synthesis. Therefore, short phosphorylated peptides, e.g., peptide L803-mts[15] and NTptide-8,[12] could function as competitive inhibitors with the primed substrates of GSK3β. The use of phosphorylated peptide inhibitors is suitable for the long-term treatment of diabetes, without the potential to be oncogenic. This is in contrast to ATP-competitive inhibitors, which prevent the phosphorylation of every substrate and subsequently elevate the level of β-catenin. Insights into the mechanism of GSK3β binding to primed substrates are beneficial to design and development of competitive GSK3β inhibitors.

The three-dimensional (3D) structure of the GSK3β in complex with the primed substrate, however, is experimentally unavailable to date. This prevents further understanding of the P+4 primed phosphorylation mechanism of the substrates. Ilouz et al.[16] have constructed a 3D model of GSK3β and the phosphorylated cAMP responsive element binding protein (pCREB), using a protein−protein docking method. Several residues interacting with the pCREB have identified via site-directed mutagenesis and biological studies. However, the molecular basis for the primed phosphorylation specificity for GSK3β substrates is obscure.

In this study, the unique P+4 primed phosphorylation specificity is examined by molecular modeling and MD simulations. First, a 3D model structure of the ternary complex of GSK3β, ATP, and the pGS peptide (GSK3β/ATP/pGS) is built by molecular modeling. The constructed model explains why the P-site in the consensus phosphorylation sequence recognized by GSK3β, SXXXS(p), is strictly separated by three residues. Then, comparative MD simulations on the systems GSK3β/ATP/pGS and GSK3β/ATP/GS are carried out. The latter system lacks a phosphate group bound to the P+4 serine of GS. The simulations address the following issue: (1) The inability of phosphorylation to induce the active conformation of the GSK3β when the pGS phosphoserine residue binds to GSK3β. (2) The fundamental basis of the primed phosphorylation mechanism.

MATERIALS AND METHODS

Molecular Modeling of the Ternary GSK3β/ATP/pGS Complex. The 2.4 Å crystal structure of GSK3β complexed with the nonhydrolyzable ATP analog adenyl imidodiphosphate, AMP (PDB ID: 1PYX[17]), was extracted from the RCSB Protein Data Bank (PDB).[18] The crystal structure of GSK3β is a dimer. However, the substrate binding site is obstructed by dimerization, so that the dimer would be inactive in heterophosphorylation.[13] The superimpositions of the dimer (PDB ID: 1PYX[17]) and monomer (PDB ID: 1O9U[19]) crystal structures of GSK3β reveal that the rmsd value between the two structures is small, with the value of 0.92 Å, indicating that the conformations for the dimer and monomer crystal structures of GSK3β are similar. Moreover, the superimpositions of the active site residues (Lys85, Asp132, Val135, Asp181, Lys183,

Asn186, and Asp200), responsible for the catalytic reaction, between the dimer and the monomer crystal structures reveal that the alignment of the active site residues is similar, with the rmsd value of 0.42 Å. In addition, to date, there is only one solved GSK3β complexed with the ATP analogue, AMP, (PDB ID: 1PYX[17]) available in the PDB. Considering that the conformations for the dimer and monomer crystal structures of GSK3β are similar, it is appropriate to use the one molecule of 1PYX, i.e. the chain A of 1PYX, for study. The missing residues on the two disordered loops (from Gly120 to Asp124 and from Asn287 to Glu290) of the crystal structure were determined using the Loop Search module of the Sybyl6.8[20] program. The inactive AMP was then replaced by ATP.

The superimpositions of the main-chain atoms of 1PYX[17] and the phosphorylated Tyr216 (p-Tyr216) of GSK3β (PDB ID: 1O9U[19]) were done to model the structure of the phosphorylated p-Tyr216/GSK3β/ATP binary complex, using the homology module of Discovery Studio 1.1 (Accelrys, San-Diego, CA). The side-chain conformation of Tyr216 in 1PYX[17] was modified to match that of p-Tyr216 in 1O9U.[19] The structure of the phosphorylated p-Tyr216/GSK3β/ATP complex was then superimposed with the crystal structure of GSK3β complexed with a phosphate ion (PDB ID: 1I09[14]). The coordinates of the phosphate ion in 1I09[14] was extracted and merged into the priming phosphate binding site of the p-Tyr216/GSK3β/ATP complex.

The structure of p-Tyr216/GSK3β/ATP complexed with the phosphate ion was finally superimposed on the X-ray structure of the p-Thr160/CDK2/cyclin A/substrate peptide/ATP analog complex (PDB ID: 1QMZ[4]) to model the p-Tyr216/GSK3β/ATP/phosphorylated substrate complex. The substrate, HHASPRK in the CDK2 catalytic site, was then used as a template for modeling a portion of the 8-amino acid GS peptide (sequence RHSSPHQSp) according to the following sequence alignment, as previously reported by Bax et al.[21] [The N- and C-termini of GS were capped by acetyl (ACE) and N-methyl (NME) groups, respectively.]

CDK2 substrate HHASPRK

GSK3β substrate ACE-RHSSPHQSp-NME

The terminal phosphate of p-Ser in p-GS was positioned to superimpose with the phosphate ion in the priming phosphate binding site, and the coordinates of the phosphate ion were then ruled out from the complex; the resulting initial model of the ternary p-Tyr216/GSK3β/ATP/pGS complex was obtained.

Energy minimization of the obtained model was carried out using the Simulation module Discovery Studio 1.1 with the CHARMM force field.[22] First, GSK3β, ATP, P serine, and the P+4 p-Ser of pGS were fixed, and the model was minimized until a convergence of 0.01 kcal/mol/Å was reached by steepest descent. Afterward, GSK3β and ATP were fixed, and the model was subjected to molecular mechanics optimization using a conjugated gradient. Finally, all the restraints were released in the last energy minimization. The optimized model was used in the subsequent MD simulations.

MD Simulations. MD simulations were conducted on the systems p-Tyr216/GSK3β/ATP/pGS and p-Tyr216/GSK3β/ATP/GS, which differ in the phosphate group bound to the GS P+4 serine. A standard AMBER FF03[23,24] force field was placed on the kinase and substrate. The force field parameters for the p-Tyr216 of GSK3β, the P+4 p-Ser of pGS (with a −2 charge), and ATP (−4 charge) were obtained from the AMBER parameter database.[25] Default protonation states at pH 7 were set for the ionizable residues. For the histidine residues, calculations of the local electrostatic environment with PROPKA[26] indicate that His106, His145, and His299 of GSK3β, and P-2 His of pGS were protonated at N_δ (delta protonation), whereas His173, His179, and His381 of GSK3β, and P+2 His of pGS were protonated at N_ε (epsilon protonation). Hydrogen atoms were assigned to the heavy atoms using the Xleap module in the AMBER9 package.[27] Each system was embedded in the truncated octahedron box of the TIP3P[28] water molecules with an 8.0 Å buffer. An appropriate number of Cl^- counterions was added to maintain the electroneutrality of each system. This was done by random substitution of water molecules with ions at the most favorable electrostatic potential positions. About 39,660 atoms were used for each system.

Energy minimizations and MD simulations were performed for each system using the SANDER module of the AMBER9 package. First, energy minimization of the water molecules and counterions with a positional restraint of 500 kcal mol^{-1} $Å^{-2}$ in the complex was performed to remove the bad contacts (the steepest descent method for the first 2000 steps and then the conjugated gradient method for the subsequent 3000 steps). Afterward, the whole system was minimized without any restraint (the steepest descent method for the first 4000 steps and then the conjugated gradient method for the subsequent 6000 steps). After relaxation, each system was gradually heated from 0 to 150 K and then from 150 to 300 K in 10 ps. This was followed by constant temperature equilibration at 300 K for 300 ps, with a positional restraint of 10 kcal mol^{-1} $Å^{-2}$ in the complex in a canonical ensemble (NVT). Finally, 12 ns MD simulations were carried out on both systems in an isothermal isobaric ensemble (NPT) with periodic boundary conditions. An integration step of 2 fs was set for the MD simulations, and the long-range electrostatic interactions were treated by the particle mesh Ewald method,[29] using a cubic fourth-order B-spline interpolation, and by setting the direct sum tolerance to 10^{-5}. A cutoff equal to 10 Å was used for short-range electrostatics and van der Waals interactions. The SHAKE method,[30] with a tolerance of 10^{-5} Å, was applied to constrain all covalent bonds involving hydrogen atoms. The temperature and pressure were coupled with a time constant of 1.0 ps and isotropic position scaling and a relaxation time of 2.0 ps by the Langevin's algorithm.[31] The coordinates were saved every 1.0 ps for analysis.

MM-GBSA Calculation. A total of 101 snapshots were extracted from the last 1 ns trajectory with an interval of 10 ps for each system. The water molecules and counterions were stripped. The molecular mechanics generalized Born/surface area (MM-GBSA) method[32,33] was used to calculate the relative free energies of substrate binding to GSK3β. Generally, the GSK3β-substrate binding free energy ($\Delta G_{binding}$) was calculated using eq 1

$$\Delta G_{binding} = \Delta G_{complex} - [\Delta G_{GSK3\beta} + \Delta G_{substrate}] \quad (1)$$

where $\Delta G_{complex}$, $\Delta G_{GSK3\beta}$, and $\Delta G_{substrate}$ are the free energies of the complex, GSK3β, and the substrate, respectively. Each free energy term in eq 1 was computed as a sum of the absolute free energy in the gas phase (ΔE_{gas}), the solvation free energy ($\Delta G_{solvation}$), and the entropy term ($T\Delta S$), using eq 2

$$\Delta G_{binding} = \Delta E_{gas} + \Delta G_{solvation} - T\Delta S \quad (2)$$

ΔE_{gas} was expressed as the sum of changes in the van der Waals energy (ΔE_{vdW}), electrostatic energy (ΔE_{ele}), and internal energies (ΔE_{int}) in the gas phase [eq 3]

$$\Delta E_{gas} = \Delta E_{vdW} + \Delta E_{ele} + E_{int} \quad (3)$$

The solvation free energy, $\Delta G_{solvation}$, estimated using continuum solvent methods, can be partitioned into two parts [eq 4]: the polar contribution (ΔG_{GB}) and the nonpolar contribution ($\Delta G_{nonpolar}$)

$$\Delta G_{solvation} = \Delta G_{GB} + \Delta G_{nonpolar} \quad (4)$$

$$\Delta G_{nonpolar} = \gamma \times SASA + b \quad (5)$$

The polar contribution (ΔG_{GB}) to the solvation energy was calculated using the GB model (Onufriev's GB, IGB = 2), as implemented in SANDER. The dielectric constants used for the interior (solute) and exterior (water) were 1 and 80, respectively. Atomic radii and charges were the same as those used in the MD simulations. The nonpolar contributions ($\Delta G_{nonpolar}$) were calculated using the function of the solvent accessible surface area (SASA), which is determined using the linear combination of pairwise overlaps;[34] the probe radius was 1.4 Å, γ = 0.0072 kcal/(mol•Å^{-2}), and b = 0 kcal/mol [eq 5]. The solute entropy contributions to the binding free energy were not computed in this work because of the extremely long durations of normal-mode analysis for large systems. Estimation of energies in this manner has proven successful in previous work[35,36] and in other studies.[37−39]

Electrostatic Potential Surface Calculation. Electrostatic potential surfaces for GSK3β and GSK3β-substrate systems obtained from the last frames from the MD simulations were calculated using the Electrostatic Potential module, as implemented in the Discovery Studio package. This was done by running Delphi,[40] a program that uses a two-dielectric implicit method and a finite difference method to solve the Poisson−Boltzmann equation to calculate the spatial distribution of the electrostatic potential and potential of the protein atoms. The default parameters were used in the calculations.

RESULTS AND DISCUSSION

GS is a GSK3β substrate that has five known P-sites in the native enzyme (designated as sites 640, 644, 648, 652, and 656), which are separated by three residues. The C-terminus Ser656 of GS is first prephosphorylated by casein kinase 2 (CK2),[41] and the other four P-sites (652, 648, 644, and 640) are then phosphorylated sequentially by GSK3β. Phosphorylation of the site Ser656 by CK2 creates the recognition site. Afterward, each successive phosphorylation modulated by GSK3β generates a new recognition site until the five P sites of the GS are phosphorylated. This is called primed phosphorylation and is about 2−3 orders of magnitude larger than phosphorylation without priming.[42] In this study, a minimal C-terminal peptide sequence containing the GS phosphorylation motif, pGS (RHSSPHQSp), is used to model the GSK3β-substrate interaction.

Molecular Modeling of the Ternary Complex p-Tyr216/GSK3β/ATP/pGS. The 3D structure of GSK3β most closely resembles that of P38γ (PDB ID: 1CM8[11]). However, there is no structure of the complex P38γ-substrate. Thus, the structure of the activated substrate-bound CDK2 (PDB ID: 1QMZ[4]) is used as a template to construct the GSK3β-substrate complex, wherein the sequence of GSK3β is 41% similar to that of CDK2.

Tyr216, a GSK3β P-site in the A loop, resides in a similar position as p-Thr185 of P38γ. The phenol side chain of unphosphorylated Tyr216 in 1PYX[17] protrudes into the primed substrate binding groove and blocks access to the binding of primed substrates (Figure 1). When phosphorylated, it moves out of the groove, as evidenced in the p-Tyr216 structure of GSK3β (PDB ID: 1O9U[19]) and increases the catalytic activity of GSK3β by ∼5-fold.[19] The A loop of the two structures, 1PYX[17] and 1O9U,[19] however, differs only slightly in the side-chain conformation of Tyr216. Here, the p-Tyr216 GSK3β/ATP model is built by modifying the side chain conformation of Tyr216 in 1PYX[17] to match that of p-Tyr216 in 1O9U.[19]

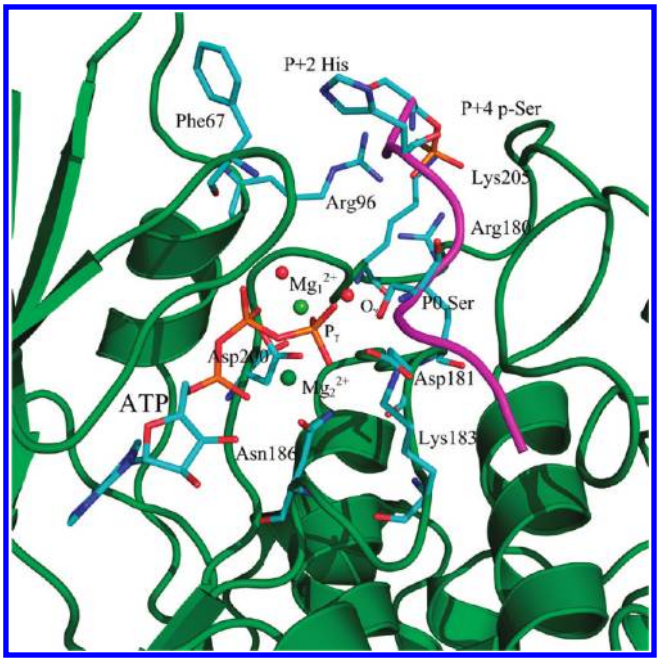

Figure 2. Model structure of the ternary complex GSK3β/ATP/pGS. The phosphorylated substrate (pGS) is in an extended conformation across the catalytic groove on the surface of the GSK3β and shown in magenta. ATP is shown as a stick model. Two Mg^{2+} ions and the water molecules are depicted by the green and red spheres, respectively. Residues Phe67, Arg96, Arg180, Asp181, Lys183, Asn186, and Lys205 of GSK3β and residues P-site serine, P+2 His, and P+4 p-Ser (phosphorylated serine) of pGS are shown in stick models and colored according to atom types (C, N, O, and P shown in cyan, blue, red, and orange, respectively). The same color scheme is used in all of the figures. For clarity, the hydrogen atoms are omitted.

The structure of the complex p-Tyr216/GSK3β/ATP/pGS (GSK3β/ATP/pGS hereafter) is shown in Figure 2. The 8-amino acid substrate derived from the optimized structure of pGS binds in an extended conformation across the catalytic groove on the surface of the kinase and interacts with the N- and C-terminal domains of GSK3β, specifically with the priming phosphate binding site. The serine at the P0 site of pGS is directed toward the γ-phosphate of ATP. The distance S_0-O_γ...P_γ-ATP between the P-site serine hydroxyl group (terminal O_γ atom) of pGS and the ATP terminal γ-phosphate group (P_γ atom) is 3.01 Å. The Mg_1^{2+} ion is octahedrally coordinated by oxygen atoms from the ATP phosphate moiety ($O_{\beta 2}$ and $O_{\gamma 3}$ atoms), the invariant residue Asp200 ($O_{\delta 1}$ and $O_{\delta 2}$ atoms), and two oxygen atoms from water molecules. The Mg_2^{2+} ion, however, is tetrahedrally coordinated by oxygen atoms from the ATP phosphate moiety ($O_{\alpha 2}$ and $O_{\gamma 2}$ atoms), Asn186 $O_{\delta 2}$, and Asp200 $O_{\delta 2}$ oxygen atoms. The two cofactor Mg^{2+} ions help the ATP to adopt an active conformation for proper phosphoryl-transfer. The substrate peptide serine at the P0 site (P-site) is hydrogen bonded with the conserved residues Lys183 and Asp181. QM/MM calculations by Cheng et al.[43] indicate that the conserved Asp166

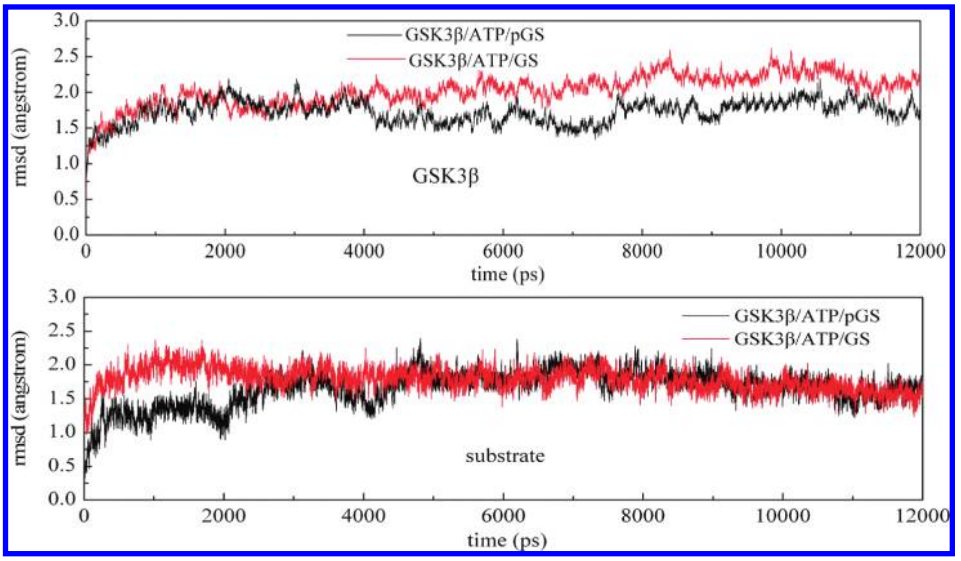

Figure 3. The time dependence of rmsds from the minimized structure for the Cα atoms of GSK3β (upper) and substrate (lower) for the GSK3β/ATP/pGS system (black) and GSK3β/ATP/GS system (red) in the 12 ns MD simulations.

(corresponding to Asp181 in GSK3β) in PKA serves as the catalytic base to accept the proton from the serine at the P-site of the substrate. In CDK2, data of De Vivo et al.[44] suggest that Asp127 does not act as the general base but keeps the substrate serine in the near-attack reactive conformation during the reaction mechanism. Thus, the role of the conserved catalytic Asp residue in the protein kinases depends on the protein environment.

In the C-terminus of the substrate, the p-Ser at the P+4 position of pGS forms hydrogen-bonding and electrostatic interactions with the triad of positive residues: Arg96 from the helix αC of N-terminus, Arg180 from the catalytic loop, and Lys205 from the A loop. The location of the p-Ser in the GSK3β-substrate model is in the same position as the p-Thr in P38γ, CDK2, and PKA. The interactions between the p-Ser and the triad optimize the orientation of the N- and C-terminal domains of GSK3β. The detailed mechanisms are described by the MD results. In addition, His at P+2 of pGS interacts with the surface-exposed Phe67 of GSK3β involved in $\pi-\pi$ interaction. Mutations of Phe to Ala impair the GSK3β phosphorylation of several substrates, including pGS.[16]

The P-site in the consensus phosphorylation sequence recognized by GSK3β, SXXXS(p), is strictly separated by three residues. Indeed, the catalytic site of GSK3β may determine a fixed distance between the P-site serine to be phosphorylated and the C-terminus p-Ser of the primed substrates. The predicted distance for the two Cα atoms between the P0 serine and the P+4 p-Ser of pGS is 11.76 Å in the model for the GSK3β-substrate complex. Modeling of the P+3 and P+5 primed phosphorylated substrates, termed SGGS(p) and SGGGGS(p), respectively, is then attempted. Here, the Gly residue is used to represent the X residue, and the distance of the two Cα atoms between the P-site serine and the C-terminus p-Ser of the substrate is measured. When the two Gly residues are used in the SGGS(p) sequence in the P+3 motif, the calculated distance for the two Cα atoms between the P0 serine and the P+3 p-Ser is 8.79 Å. This indicates that the two Gly connecting residues do not provide the adequate proximity required to position the P0 serine or the P+3 p-Ser for proper interaction with the γ-phosphate of ATP and the priming phosphate binding site of GSK3β, respectively. When four Gly residues are used in the SGGGGS(p) sequence in the P+5 motif, the calculated distance for the two Cα atoms between the P0 serine and the P+5 p-Ser is 13.90 Å; this suggests that the four Gly connecting residues are too long to connect the γ-phosphate of ATP to the priming phosphate binding site of GSK3β. Thus, the optimal distance between the P0 serine and the P+4 p-Ser of pGS in the model of GSK3β-substrate complex may explain the GSK3β recognition of the canonical phosphorylation sequence, SXXXS(p), which contains a P0 serine and a P+4 p-Ser separated by three residues.

MD Simulations. To explore the stability of the GSK3β/ATP complexes with the 8-residue peptide substrate with and without the priming phosphate group on the P+4 serine of GS, (GSK3β/ATP/pGS and GSK3β/ATP/GS, respectively), two MD simulations (12 ns) of the fully solvated complexes are performed. Analysis of the flexibility of the GSK3β, together with characterization of the GSK3β-substrate and substrate-ATP interactions, provides detailed information on the primed phosphorylation mechanism.

Protein rmsd and Flexibility. The Cα atoms rms coordinate deviations (rmsds) of the simulated GSK3β complex in relation to the initial minimized structure are shown in Figure 3. Each frame of the trajectory is superimposed on the reference using the least-squares fit method. As depicted in the upper panel of Figure 3, the rmsd value of GSK3β complexed with the primed substrate, pGS, is about 1.8 Å. In contrast, the rmsd value of GSK3β complexed with the nonprimed substrate, GS, is slightly higher, with an average value of 2.2 Å. These data show that the structure of GSK3β complexed with the nonphosphorylated GS experiences a conformational change compared with that of GSK3β complexed with the pGS. The rmsd values of pGS and GS in the corresponding systems, as shown in the lower panel of Figure 3, are similar in the simulations.

The flexibility of the simulated systems can be acquired from the B-factors (B), which are directly related to the mean square atomic fluctuations $<R^2>$. B is calculated by eq 6, which uses the X-ray data and their differences among the simulated systems

$$B = (8\pi^2/3) < R^2 > \quad (6)$$

dx.doi.org/10.1021/ci100493j |J. Chem. Inf. Model. 2011, 51, 1025–1036

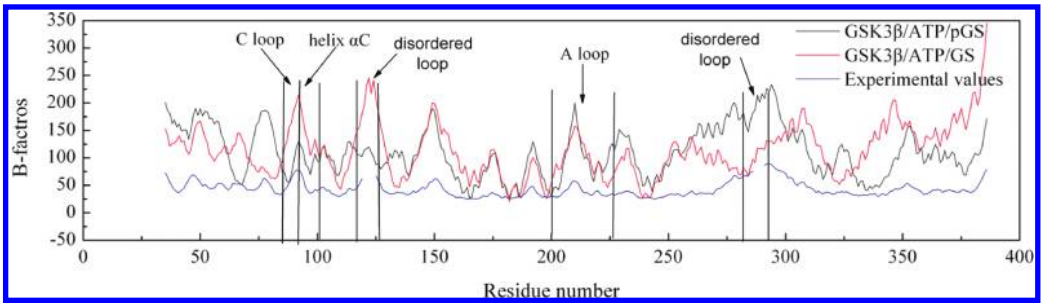

Figure 4. Calculated B-factors for the GSK3β/ATP/pGS system (black) and GSK3β/ATP/GS system (red) and the experimental B-factors (blue) for the Cα atoms of GSK3β (PDB code 1PYX). The calculated value was averaged over 12 ns time frames in the MD simulations.

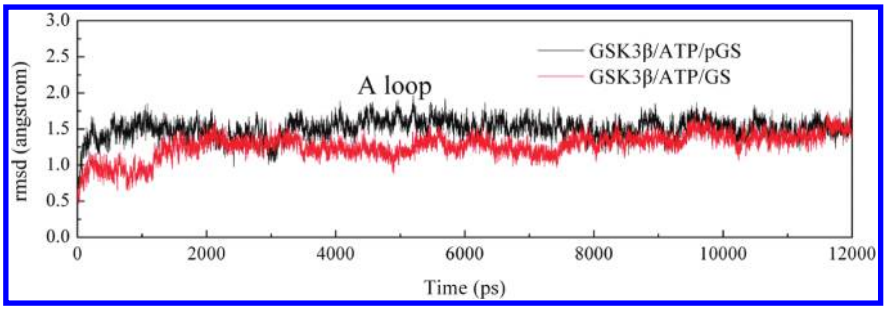

Figure 5. The time dependence of rmsds for the A loop of GSK3β in the two simulated systems during the 12 ns MD simulations.

Figure 4 shows the two calculated B-factors for the GSK3β/ATP/pGS and GSK3β/ATP/GS systems as well as the experimental B-factors for the Cα atoms of the GSK3β. The correlation coefficients between the predicted and experimental B-factors for GSK3β/ATP/pGS and GSK3β/ATP/GS are 0.723 and 0.518, respectively. These indicate a better fit between the experimental and the predicted flexibility for the GSK3β/ATP/pGS system compared with that for the GSK3β/ATP/GS system. Overall, the data show relatively similar fluctuation patterns for the two systems except for the missing residues on the two disordered loops. However, residues 89−95 in the loop, named the C loop, preceding the helix αC and residues 96−102 (helix αC) of the N-terminal lobe exhibit a much higher flexibility in the GSK3β/ATP/GS system compared with those in the GSK3β/ATP/pGS system. The average B-factor values are 148.68 and 99.17 Å^2, respectively. Of particular interest is that the predicted B-factor values are similar for residues 200−226 in the two systems (corresponding to the A loop) with the average B-factor values of 97.68 and 96.07 Å^2, respectively. The B-factors together with the rmsds for the A loop (Figure 5) demonstrate that the conformation of the A loop is similar in the two systems, regardless of the phosphorylated state of the substrate. This indicates that the active conformation of GSK3β is not induced by phosphorylation, consistent with the experimental results.[14] In contrast, in P38γ, CDK2, and PKA, the active conformation of the kinase is induced by the phosphorylation of the A loop.

Average Structures and Electrostatic Potential Calculations. The average structures are calculated by averaging coordinates from the 12 ns collective trajectories. The superimpositions of the backbone atoms of the X-ray structures on the average structures of GSK3β/ATP/pGS and GSK3β/ATP/GS reveal that the primed substrate induces a closed conformation of the C loop and the β-turn secondary structure of the A loop, whereas the open conformation is presented in the nonprimed substrate system (Figure 6). This dynamic behavior is in agreement

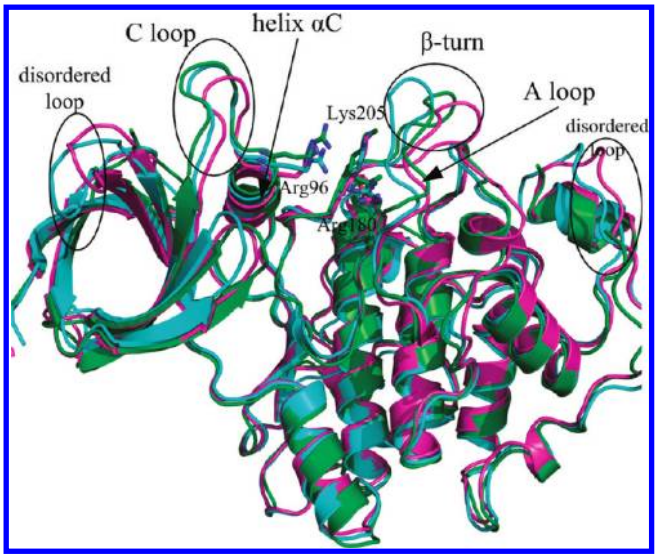

Figure 6. The superimpositions of the backbone atoms of the X-ray structure (green) on the average structures obtained from the MD simulations corresponding to the GSK3β/ATP/pGS (cyan) and GSK3β/ATP/GS systems (magenta).

with previous studies on the GSK3β/ATP/p-Ser systems.[45] The distance between the Cα atoms of the two residues Arg92 and Gly210 at the apex of the respective C loop and β-turn is shown in Figure 7. An opening motion of the GSK3β structure in the GSK3β/ATP/GS system is observed during the MD simulation. For example, the distance begins to increase at the 4 ns and reaches about 28 Å along the remaining MD simulation in the GSK3β/ATP/GS system. In contrast, the distance in the GSK3β/ATP/pGS system fluctuates around 20 Å most of the time after the 4 ns MD simulation, except in the period between 7 and 10 ns.

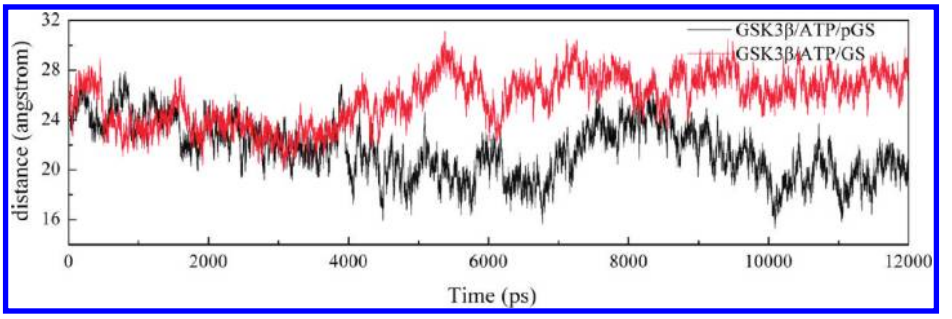

Figure 7. The distance between the two Cα atoms of residues Arg92 and Gly210 in the two simulated systems.

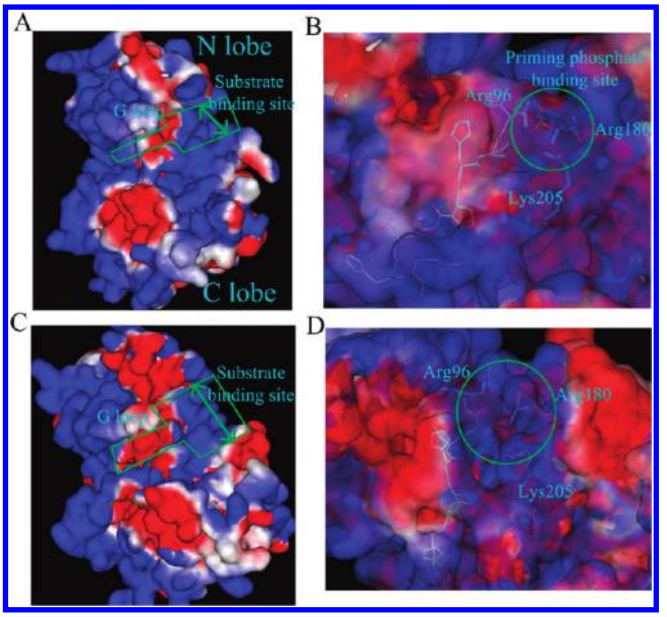

Figure 8. Electrostatic potential analyses. (A) Electrostatic potential surface on GSK3β in the GSK3β/ATP/pGS system with the substrate pGS removed. (B) Electrostatic potential for the GSK3β/ATP/pGS complex, visualized in the context of the molecular structure. (C) Electrostatic potential surface on GSK3β in the GSK3β/ATP/GS system with the substrate GS removed. (D) Electrostatic potential for the GSK3β/ATP/GS complex and visualized in the context of the molecular structure. Electrostatic potentials are color coded: positive charges are in blue, negative charges are in red, and neutral residues are in white.

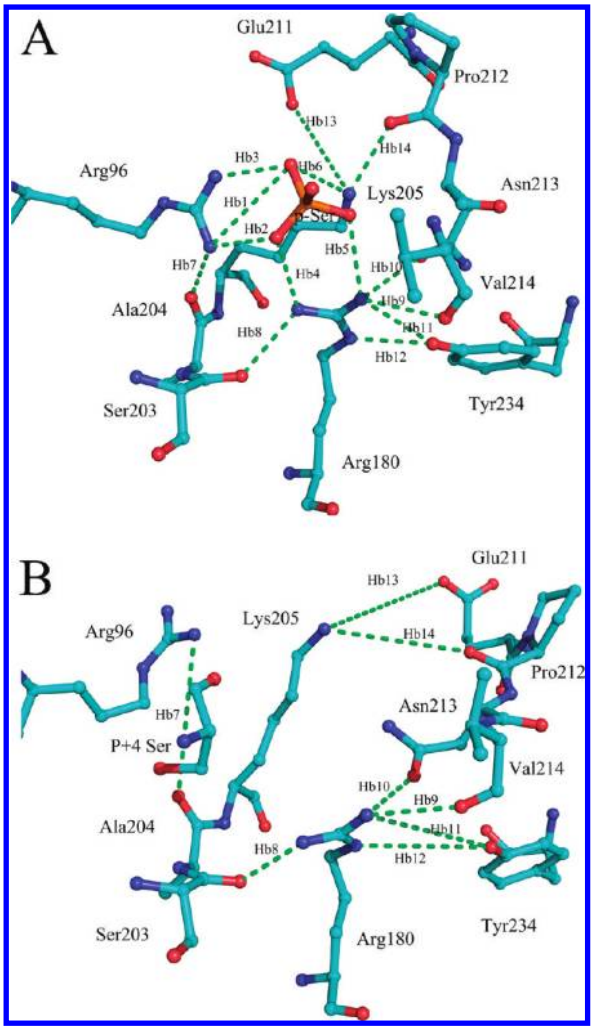

Figure 9. Hydrogen-binding network around the triad of positive residues in the GSK3β/ATP/pGS (A) and GSK3β/ATP/pGS (B) systems.

Electrostatic interactions between the GSK3β and the primed substrates are generally considered as the main driving force in the recognition of primed substrates. Here, the contribution of electrostatic interactions in the stabilization of the two systems is explored. The last frames from the MD simulations are investigated by means of the Delphi program[40] implemented in the Discovery Studio package, and electrostatic potential surfaces are separately calculated for the complexes and the GSK3β in the binding conformation extracted from the MD complexes. As shown in Figure 8A, the electrostatic potential for the priming phosphate binding site (consisting of the residues Arg96, Arg180, and Lys205) in the GSK3β obtained from the GSK3β/ATP/pGS system is strongly positive. Thus, the negative priming phosphate group of the primed substrate is needed to occupy the positive phosphate binding site to compensate for the cluster of positively charged residues. This is consistent with the function of the phosphate group of the A loop p-Thr occupying the phosphate binding site in P38γ, CDK2, and PKA. As a result, the compact conformation of the priming phosphate binding site is formed (Figure 8B), with the cavity volume comprising the triad of positive residues of about 250 Å^3. The conformations of the triad are consequently pivotal for the correct alignment of the N- and C-terminal domains of GSK3β. On the contrary, when the hydroxyl group of the GS P+4 serine occupies the phosphate

dx.doi.org/10.1021/ci100493j |J. Chem. Inf. Model. 2011, 51, 1025–1036

Table 1. Summary of the Average Distances between Heavy Atoms (Å) and Percent of Occurrence Data for Important Hydrogen Bonding Interactions Surrounding the Triad of Positive Residues in the Two Simulated Systems

		GSK3β/ATP/pGS		GSK3β/ATP/GS	
number	H-bond	X···Y	%	X···Y	%
Hb1	Arg96-NH1···O1P-pSer	3.218 ± 0.20	60.30	/	0
Hb2	Arg96-NH1···O2P-pSer	2.848 ± 0.16	98.31	/	0
Hb3	Arg96-NH2···O1P-pSer	2.794 ± 0.11	99.93	/	0
Hb4	Arg180-NH1···O2P-pSer	2.779 ± 0.11	98.58	/	0
Hb5	Arg180-NH2···O3P-pSer	2.803 ± 0.13	99.39	/	0
Hb6	Lys205-NZ···O1P-pSer	2.787 ± 0.12	94.66	/	0
Hb7	Arg96-NH1···O-Ala204	2.953 ± 0.17	91.90	2.953 ± 0.18	45.45
Hb8	Arg180-NH1···O-Ser203	2.826 ± 0.11	99.73	2.856 ± 0.13	99.75
Hb9	Arg180-NH2···O-Val214	3.129 ± 0.19	31.93	3.119 ± 0.19	65.72
Hb10	Arg180-NH2···OD1-Asn213	2.844 ± 0.14	78.68	2.950 ± 0.18	37.01
Hb11	Arg180-NH2···OH-Tyr234	3.290 ± 0.15	41.24	3.206 ± 0.18	47.42
Hb12	Arg180-NE···OH-Tyr234	3.111 ± 0.16	91.84	3.160 ± 0.17	68.09
Hb13	Lys205-NZ···OE1-Glu211	2.863 ± 0.16	59.60	2.877 ± 0.19	15.73
Hb14	Lys205-NZ···O-Pro212	2.878 ± 0.12	94.66	3.042 ± 0.20	7.26

binding site, the positive potential generated by this cluster of basic side chains is not effectively offset by the hydroxyl groups. More significantly, the interaction with Arg96 from the helix αC of the N-terminal domain, which positions the catalytic residues in their active conformation, would be hard to maintain.[13] Consequently, the C loop and the helix αC present an enhanced flexibility for the GSK3β/ATP/GS system, as observed from the B-factor calculation. The side-chain conformations of the triad move away from each other due to electrostatic repulsion. As a result, the priming phosphate binding site in the GSK3β/ATP/GS systems is presented in an open conformation (Figure 8D), with a cavity volume of about 400 Å^3. On the other hand, the coupled N- and C-terminal domains of GSK3β are disturbed by the movement of the Arg96 side chain, which leads to an open substrate binding site in the GSK3β/ATP/GS system (Figure 8C), whereas in the GSK3β/ATP/pGS system (Figure 8A), the substrate binding site is presented in a closed state. This is in accordance with the average structure analyses. The result suggests that the interactions between the two lobes loosen in the absence of a substrate phosphate group in the GSK3β/ATP/GS system. The closure of the two lobes in this system may facilitate more firm substrate binding; this provides an explanation for the increased rate of priming phosphorylation compared with phosphorylation without priming.[42]

GSK3β-Substrate and ATP-Substrate Interactions. The hydrogen-bond network formed by the p-Ser at P+4 of the pGS and the side chain groups of the triad of positive residues (Arg96, Arg180, and Lys205) is well maintained in the GSK3β/ATP/pGS system during the MD simulations. The hydrogen-bond contacts are characterized by means of average distances between the corresponding heavy atoms and by percentage of occurrence data. Specifically, p-Ser is hydrogen-bonded to Hb1@Arg96, Hb2@Arg96, Hb3@Arg96, Hb4@Arg180, Hb5@Arg180, and Hb6@Lys205 (Figure 9A and Table 1). This hydrogen-bond network in the priming phosphate binding site is in good agreement with what is obtained by the pThr160 and the three coordinated guanidinium groups of each arginine residue (Arg50, Arg126, and Arg150) during the MD simulation.[46] In contrast, none of the hydrogen bonds are observed between the serine at P+4 of GS and the positive triad in the GSK3β/ATP/GS system (Table 1). This leads to movement of the side chain groups of the triad away from their initial positions and subsequently to the open state of the phosphate binding site (Figure 9B). In addition, the other eight hydrogen bonds are formed between the side chain groups of the triad and the backbone or side chain residue atoms of the following: Hb7@Arg96 with the backbone oxygen atom of Ala204; Hb8@Arg180 and Hb9@Arg180 with the backbone oxygen atoms of Ser203 and Val214, respectively; Hb10@Arg180, Hb11@Arg180, and Hb12@Arg180 with the side chain oxygen atoms of Asn213 and Tyr234, respectively; and Hb13@Lys205 and Hb14@Lys205 with the side chain and backbone oxygen atoms of Glu211 and Pro212, respectively. Regardless of the phosphorylated state of the substrate, the Arg180 from the catalytic loop donates five hydrogen bonds to the GSK3β residues in the two simulated systems (Table 1). This, in turn, helps stabilize the active conformation of the A loop, as observed from the similar B-factor and rmsd values. Thus, the active conformation of GSK3β does not need to be induced by the primed substrates. Most remarkably, the hydrogen-bonding interactions surrounding the residues Arg96 and Lys205, observed in the GSK3β/ATP/pGS system, are lost in the GSK3β/ATP/GS system. The loss of these hydrogen bonds results in the enlargement of the priming phosphate binding site in the GSK3β/ATP/GS system. This is in agreement with a PKA study, in which the mutation of His87 (corresponding to Arg96 in GSK3β) to Ala87 is shown to effect the uncoupling of the two lobes and leads to interlobe opening.[47]

The water environment around the side-chain nitrogen atoms of the triad is further explored by computing for the radial distribution function (RDF) between the nitrogen atoms of the triad and the water molecules in the two studied systems. Figure 10 shows the RDFs derived from the MD simulations. The plots show sharp peaks centered at 2.95 Å in the triad of the GSK3β/ATP/GS system. The presence of these peaks indicates that the water molecules may have interacted with the NH1 and NH2 atoms of Arg96 and Arg180 and with the NZ atom of Lys205 in the GSK3β/ATP/GS system during MD simulations.[48] In contrast, in the GSK3β/ATP/pGS system, the probability that water molecules interacted with the triad during the MD simulations is low, as

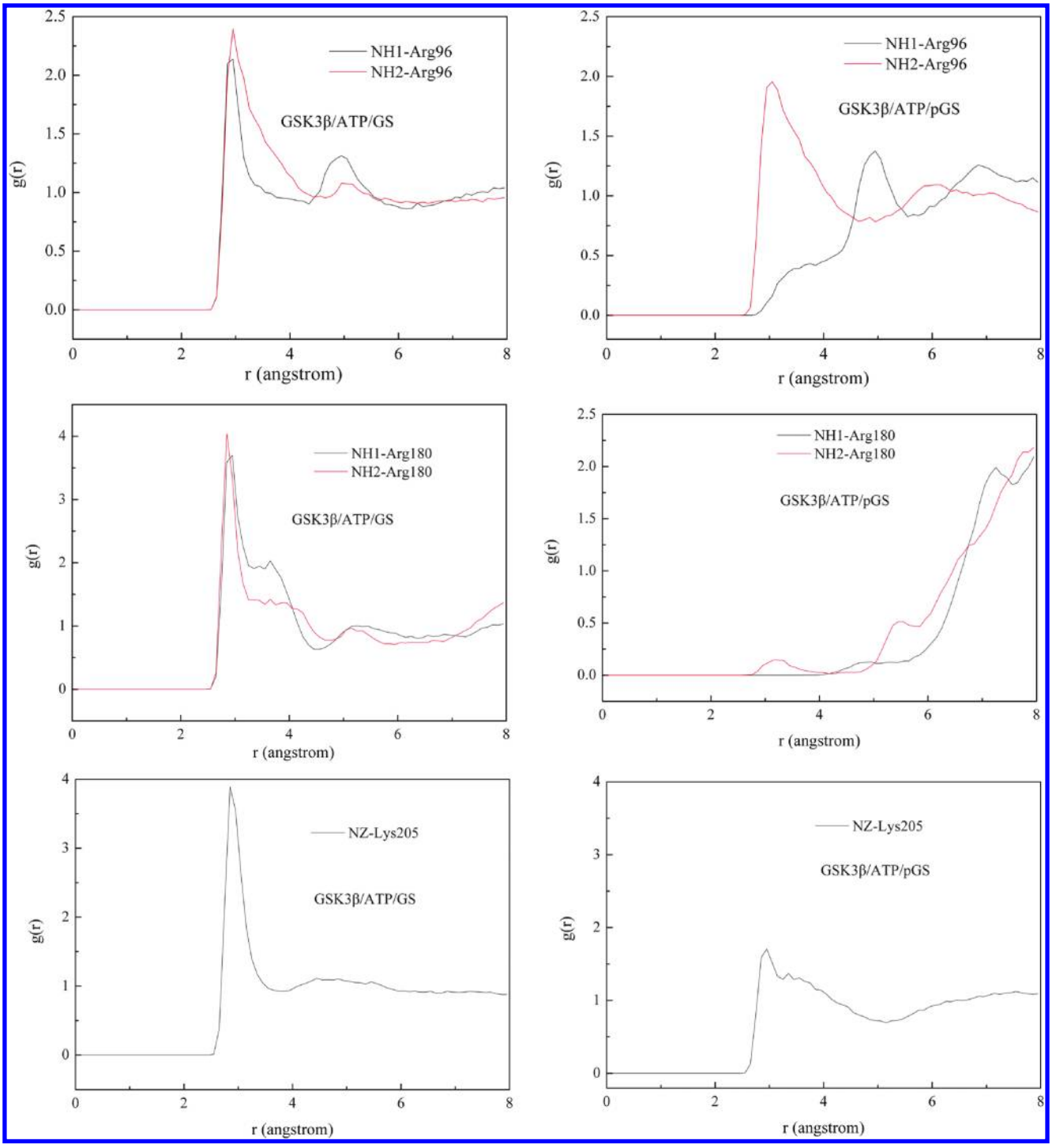

Figure 10. Water radial distribution functions for the triad in the GSK3β/ATP/pGS (right) and GSK3β/ATP/pGS (left) systems.

suggested by the fewer sharp peaks centered at 2.95 Å. These results indicate that the side chain groups of the triad in the GSK3β/ATP/GS system are surrounded by the water molecules, which partially hydrate the basic residues no longer involved in electrostatic and hydrogen-bonding interactions with the lacking phosphate of serine at the P+4 position of the substrate. This coincides with the MD simulations of unphosphorylated Thr160 CDK2.[46]

In the active site of GSK3β, the nucleophilic hydroxyl group of the P-site serine interacts simultaneously with the ATP. The distances between the entering oxygen atom and the γ-phosphorus of ATP (S_0-O_γ...P_γ-ATP) are shown in Figure 11. The calculated average distance is 3.76 $\pm$ 0.25 Å, which is compatible with the phosphor-transfer for the GSK3β/ATP/pGS system, and agrees well with the corresponding distance values of 3.75 $\pm$ 0.70 Å for CDK2,[49] 3.8 $\pm$ 0.3 Å for PKA,[50] and 3.95 $\pm$ 0.46 Å for PAK1.[51] In contrast, the average distance for S_0-O_γ...P_γ-ATP for the GSK3β/ATP/GS system is equal to 5.04 $\pm$ 0.48 Å in the MD simulation, which is beyond the threshold for a hydrogen bond. Therefore, the S_0-O_γ...P_γ-ATP distance in the primed substrate is largely shortened compared with that in the nonprimed substrate, and a very strong

dx.doi.org/10.1021/ci100493j |J. Chem. Inf. Model. 2011, 51, 1025–1036

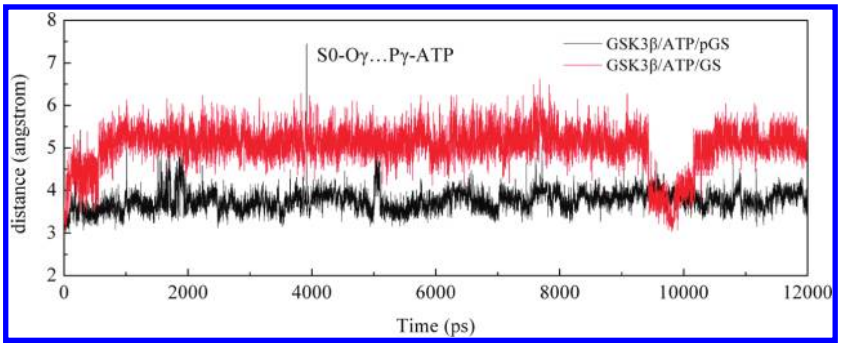

Figure 11. The time dependence of the reaction coordinate distance S_0-O_γ...P_γ-ATP in the two systems simulated by MD.

Table 2. Free Energy Terms (kcal/mol) in the Calculation of Binding Free Energies of GSK3β and the Substrate in the GSK3β/ATP/pGS and GSK3β/ATP/GS Systems[a]

complex	ΔE_{ele}	ΔE_{vdW}	ΔG_{GB}	ΔG_{np}	$\Delta G_{GB,ele}$	ΔG_{bind}
GSK3β/ATP/pGS	−471.53(25.50)	−23.53(6.18)	443.82(20.63)	−7.19(0.67)	−27.71(8.84)	−58.43(5.62)
GSK3β/ATP/GS	−75.59(19.82)	−50.09(4.63)	99.03(14.66)	−10.30(0.46)	23.44(8.08)	−36.95(8.88)

[a] Values in parentheses are standard deviations. ΔE_{int} is not included here, since it is equal to zero in the single trajectory approach. $\Delta G_{GB,ele}$ is the sum of changes in the gas phase electrostatic energy and the polar solvation free energy, $\Delta E_{ele} + \Delta G_{GB}$.

hydrogen bond with the serine hydroxyl group is established. The significant decrease in the reaction coordinate distance in the GSK3β/ATP/pGS system facilitates the phosphoryl-transfer reaction.

Free Energies of Binding. Free energies of binding ($\Delta G_{binding}$) (Table 2) are computed using the ensembles of structures collected along the last 1 ns of the MD trajectories. The total electrostatic interactions ($\Delta G_{GB,ele}$) between the GSK3β and the substrate in the GSK3β/ATP/pGS and GSK3β/ATP/GS systems, which are composed of the gas phase electrostatic energy (ΔE_{ele}) and the polar solvation free energy contributions (ΔG_{GB}), are −27.71 and 23.44 kcal/mol, respectively. This is in accordance with the strong electrostatic and hydrogen-bonding interactions between the priming phosphate group of the pGS and the positive triad in the GSK3β/ATP/pGS system. Due to these strong interactions, ΔG_{GB} of the GSK3β/ATP/pGS system is significantly larger compared with that of the GSK3β/ATP/GS system, with a value of 443.82 and 99.03 kcal/mol, respectively. This means that less desolvation energy is needed for the unphosphorylated serine of the substrate to enter into the priming phosphate binding site. Inspection of the $\Delta E_{ele} + \Delta G_{np}$ contributions clearly shows that the van der Waals/nonpolar interactions also facilitate the binding of the substrate to the GSK3β. The total $\Delta G_{binding}$ for the GSK3β/ATP/pGS system is −58.43 kcal/mol, which is 21.48 kcal/mol lower than that of the GSK3β/ATP/GS system. This shows that the GSK3β/ATP/GS system yields a low energy-favorable complex that would consequently result in the weak binding of the nonprimed substrate to the GSK3β, which is not efficient for the phosphorylation of the nonprimed substrate.

To get an in-depth view of the effects of the phosphorylated state of the substrate on the binding affinity, a per-residue decomposition of the total energy is performed to explore the energetic differences of critical residues on the binding of the substrate. Figure 12 shows the energy contributions of the GSK3β residues for the two systems. Compared with the GSK3β/ATP/GS system, major favorable energy contributions originate predominantly from Arg96, Arg180, Lys205, and Val214 of GSK3β in the GSK3β/ATP/pGS system.

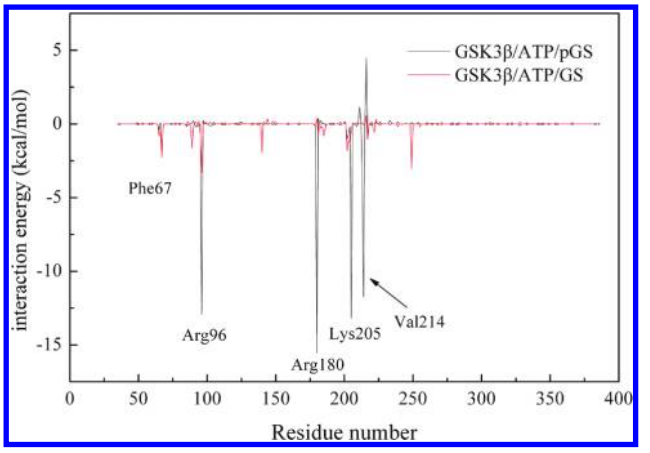

Figure 12. Contributions of individual amino acid residues of GSK3β to the binding free energies (in kcal/mol) for the two systems.

CONCLUSIONS

The unique P+4 primed phosphorylation specificity for GSK3β substrates is examined by performing a series of molecular modeling, comparative MD simulations, and MM-GBSA free energy calculations. According to the constructed 3D model of the GSK3β/ATP/pGS complex, the phosphorylated substrate pGS binds in an extended conformation across the catalytic groove on the surface of the GSK3β. The fixed distance between the P0 serine and the P+4 p-Ser of pGS can only accommodate exactly three residues. Thus, the canonical phosphorylation sequence recognized by GSK3β, SXXXS(p), contains a P0 serine and a P+4 p-Ser strictly separated by three residues.

In addition, a more detailed P+4 primed phosphorylation mechanism for GSK3β substrates is delineated based on the results of comparative MD simulations. The results reveal that the flexibility of the A loop in the two simulated systems is similar, as calculated from the B-factors and the rmsds. Thus, the active conformation of the GSK3β is not induced by phosphorylation,

which is consistent with experimental results. However, in the absence of a phosphate group, the positive potential generated by the cluster of three basic side chains cannot be adequately neutralized in the GSK3β/ATP/GS system. Subsequently, the side chains of the positive triad move away from their initial positions, and the priming phosphate binding site is presented in the open state. The hydrogen-bonding networks surrounding the triad, especially Arg96 and Lys205, are disrupted. As a result, the proper alignment of N- and C-terminal domains of the GSK3β is disturbed, as visualized from the distributions of electrostatic potentials on the molecular surface of the GSK3β/ATP/GS system. In contrast, the compact conformations of the triad in the GSK3β/ATP/pGS system are presented, and the hydrogen-bonding networks surrounding the three residues are well maintained. Consequently, the proper alignment of the N- and C-terminal domains of the GSK3β facilitates the phosphoryl-transfer reaction. Moreover, the reaction coordinate distance S_0-O_γ...P_γ-ATP is shorter in the GSK3β/ATP/pGS system compared with that in the GSK3β/ATP/GS system. Additionally, results obtained from MM-GBSA calculations reveal that the priming phosphate binding site serves as a docking site for interaction with the primed substrates to promote the binding affinity. These results may explain why GSK3β has a unique P+4 primed phosphorylation specificity for its substrates. The structural and mechanistic insights derived from the present study will provide valuable insights for the future design of competitive GSK3β inhibitors.

AUTHOR INFORMATION

Corresponding Author

*Phone: +86 574 88229516. Fax: +86 574 88229516. E-mail: yjjiang@nit.zju.net.cn.

ACKNOWLEDGMENT

This work was supported by the Natural Science Foundation of China (No. 20803063), and the Agricultural Project of Ningbo (No. 2007C10011).

REFERENCES

(1) Manning, G.; Whyte, D. B.; Martinez, R.; Hunter, T.; Sudarsanam, S. The protein kinase complement of the human genome. *Science* **2002**, *298*, 1912–1934.

(2) Cohen, P. The regulation of protein function by multisite phosphorylation-a 25-year update. *Trends Biochem. Sci.* **2000**, *25*, 596–601.

(3) Ubersax, J. A.; Ferrell, J. E., Jr. Mechanisms of specificity in protein phosphorylation. *Nat. Rev. Mol. Cell Biol.* **2007**, *8*, 530–541.

(4) Brown, N. R.; Noble, M. E. M.; Endicott, J. A.; Johnson, L. N. The structural basis for specificity of substrate and recruitment peptides for cyclin-dependent kinases. *Nat. Cell Biol.* **1999**, *1*, 438–443.

(5) Zheng, J.; Knighton, D. R.; Teneyck, L. F.; Karlsson, R.; Xuong, N.-H.; Taylor, S. S.; Sowadski, J. M. Crystal structure of the catalytic subunit of c-AMP-dependent protein kinase complexed with Mg/ATP and peptide inhibitor. *Biochemistry* **1999**, *32*, 2154–2161.

(6) Emibi, N.; Rylatt, D. B.; Cohen, P. Glycogen synthase kinase-3 form rabbit skeletal muscle: separation from cylic-AMP-dependent protein kinase and phosphorylase kinase. *Eur. J. Biochem.* **1980**, *107*, 519–527.

(7) Ali, A.; Hoeflich, K. P.; Woodgett, J. R. Glycogen synthase kinase-3: properties, functions, and regulation. *Chem. Rev.* **2001**, *101*, 2527–2540.

(8) Pearl, L. H.; Barford, D. Regulation of protein kinases in insulin, growth factor, and Wnt signaling. *Curr. Opin. Struct. Biol.* **2000**, *12*, 761–767.

(9) Cohen, P.; Frame, S. The renaissance of GSK3. *Nat. Rev. Mol. Cell Biol.* **2001**, *2*, 769–776.

(10) Eldar-Finkelman, H.; Licht-Murava, A.; Pietrokovaski, S.; Eisenstein, M. Substrate-competitive GSK-3 inhibitors-strategy and implications. *Biochim. Biophys. Acta* **2010**, *1804*, 598–603.

(11) Bellon, S.; Fitzgibbon, M. J.; Fox, T.; Hsiao, H.-M.; Wilson, K. P. The structure of phosphorylated P38γ is monomeric and reveals a conserved activation-loop conformation. *Structure* **1999**, *7*, 1057–1065.

(12) Frame, S.; Cohen, P.; Biondi, R. M. A common phosphate binding site explains the unique substrate specificity of GSK3 and its inactivation by phosphorylation. *Mol. Cell* **2001**, *7*, 1321–1327.

(13) Dajani, R.; Fraser, E.; Roe, S. M.; Young, N.; Good, V.; Dale, T. C.; Pearl, L. H. Crystal structure of glycogen synthase kinase 3β: structural basis for phosphate-primed substrate specificity and autoinhibition. *Cell* **2001**, *105*, 721–732.

(14) ter Haar, E.; Coll, J. T.; Austen, D. A.; Hsiao, H.-M.; Swenson, L.; Jain, J. Structure of GSK3β reveals a primed phosphorylation mechanism. *Nat. Struct. Biol.* **2001**, *8*, 593–596.

(15) Plotkin, B.; Kaidanovich, O.; Tailior, I.; Eldar-Finkelman, H. Insulin mimetic action of synthetic phosphorylated peptide inhibitors of glycogen synthase kinas-3. *J. Pharmacol. Exp. Ther.* **2003**, *305*, 974–980.

(16) Ilouz, R.; Kowalsman, N.; Eisenstein, M.; Eldar-Finkelman, H. Identification of novel glycogen synthase kinase-3β substrate-interacting residues suggests a common mechanism for substrate recognition. *J. Biol. Chem.* **2006**, *281*, 30621–30630.

(17) Bertrand, J. A.; Thieffine, S.; Vulpetti, A.; Cristiani, C.; Valsasina, B.; Knapp, S.; Kalisz, H. M.; Flocco, M. Structural characterization of the GSK-3β active site using selective and non-selective ATP-mimetic inhibitors. *J. Mol. Biol.* **2003**, *333*, 393–407.

(18) *Protein Data Bank*; Brookhaven National Laboratory, Upton, NY; http://www.rcsb.org/pdb. Accessed October 2, 2010.

(19) Dajani, R.; Fraser, E.; Roe, S. M.; Maggie, Y.; Good, V. M.; Thompson, V.; Dale, T. C.; Pearl, L. H. Structural basis for recruitment of glycogen synthase kinase 3β to the axin-APC scaffold complex. *EMBO J.* **2003**, *22*, 494–501.

(20) *Sybyl Version 6.8*; Tripos Associates Inc.: St. Louis, MO, 2001.

(21) Bax, B.; Carter, P. S.; Lewis, C.; Guy, A. R.; Bridges, A.; Tanner, R.; Pettman, G.; Mannix, C.; Culbert, A. A.; Brown, M. J. B.; Smith, D. G.; Reith, A. D. The structure of phosphorylated GSK-3β complexed with a peptide, FRATide, that inhibits β-catenin phosphorylation. *Structure* **2001**, *9*, 1143–1152.

(22) Brooks, B. R.; Brooks, C. L., III.; Mackerell, A. D., Jr.; Nilsson, L.; Petrella, R. J.; Rous, B.; Won, Y.; Archontis, G.; Bartels, C.; Boresch, S.; Caflisch, A.; Caves, L.; Cui, Q.; Dinner, A. R.; Feig, M.; Fischer, S.; Gao, J.; Hodoscek, M.; Im, W.; Kuczera, K.; Lazaridis, T.; Ma, J.; Ovchinnikov, V.; Paci, E.; Pastor, R. W.; Post, C. B.; Pu, J. Z.; Schaefer, M.; Tidor, B.; Venable, R. M.; Woodcock, H. L.; Wu, X.; Yang, W.; York, D. M.; Karplus, M. CHARMM; the biomolecular simulation program. *J. Comput. Chem.* **2009**, *30*, 1545–1614.

(23) Duan, Y.; Wu, C.; Chowdhury, S.; Lee, M. C.; Xiong, G.; Zhang, W.; Yang, R.; Cieplak, P.; Luo, R.; Lee, T. A point-charge force field for molecular mechanics simulations of proteins. *J. Comput. Chem.* **2003**, *24*, 1999–2012.

(24) Lee, M. C.; Duan, Y. Distinguish protein decoys by using a scoring function based on new AMBER force field, short molecular dynamics simulations, and the generalized born solvent model. *Proteins* **2004**, *55*, 620–624.

(25) Homeyer, N.; Horn, A. H.; Lanig, H.; Sticht, H. AMBER force field parameters for phosphorylated amino acids in different protonation states: phosphoserine, phosphothreonine, phosphotyrosine and phosphohistidine. *J. Mol. Model.* **2006**, *12*, 281–289.

(26) Bas, D. C.; Rogers, D. M.; Jensen, J. H. Very fast prediction and rationalization of PKa values for protein-ligand complexes. *Proteins* **2008**, *73*, 765–783.

(27) Case, D. A.; Darden, T. A.; Cheatham, T. E., III.; Simmerling, C.; Wang, J.; Duke, R. E.; Luo, R.; Merz, K. M.; Pearlman, D. A.;

Crowley, M.; Walker, R. C.; Zhang, B.; Wang, S.; Hayik, A.; Roitberg, G.; Seabra, K. F.; Wong, F.; Paesani, X.; Wu, S.; Brozell, V.; Tsui, H.; Gohlke, L.; Yang, C.; Tan, J.; Mongan, V.; Hornak, G.; Cui, P.; Beroza, D. H.; Mathews, C.; Schafmeister, W. S. R.; Kollman, P. A. *AMBER 9*; University of California: San Francisco, 2006.

(28) Jorgensen, W. L.; Chandrasekhar, J.; Madura, J. D.; Impey, R. W.; Klein, M. L. Comparison of single potential function for simulating liquid water. *J. Chem. Phys.* **1983**, *79*, 926–935.

(29) Darden, T.; York, D.; Pedersen, L. Particle mesh Ewald: an N log(N) method for Ewald sums in large systems. *J. Chem. Phys.* **1993**, *98*, 10089–10094.

(30) Ryckaert, J. P.; Ciccotti, G.; Berendsen, H. J. C. Numerical integration of the cartesian equations of motion of a system with constraints: molecular dynamics of n-alkanes. *J. Comput. Phys.* **1977**, *23*, 327–341.

(31) Wu, X.; Brooks, B. R. Self-guided Langevin dynamics simulation method. *Chem. Phys. Lett.* **2003**, *381*, 512–518.

(32) Kollman, P. A.; Massova, I.; Reyes, C.; Kuhn, B.; Shuanghong, H.; Chong, L.; Case, D. A.; Cheatham, T. E., III. Calculating structures and free energies of complex molecules: combining molecular mechanics and continuum models. *Acc. Chem. Res.* **2000**, *33*, 889–897.

(33) Wichapong, K.; Lawson, M.; Pianwanit, S.; Kokpol, S.; Sippl, W. Postprocessing of protein-ligand docking poses using linear response MM-PB/SA: Application to Wee1 kinase inhibitors. *J. Chem. Inf. Model.* **2010**, *50*, 1574–1588.

(34) Weiser, J.; Shenkin, P. S.; Still, W. C. Approximate atomic surfaces from linear combinations of pairwise overlaps (LCPO). *J. Comput. Chem.* **1999**, *20*, 217–230.

(35) Sun, H.; Jiang, Y.-J.; Yu, Q.-S.; Luo, C.-C.; Zou, J.-W. Effect of mutation K85R on GSK3β: Molecular dynamics simulation. *Biochem. Biophys. Res. Commun.* **2008**, *377*, 962–965.

(36) Zhang, N.; Jiang, Y.; Zou, J.; Zhuang, S.; Jin, H.; Yu, Q. Insights into unbinding mechanisms upon two mutations investigated by molecular dynamics study of GSK-3β-Axin complexes: role of packing hydrophobic residues. *Proteins* **2007**, *67*, 941–949.

(37) Wang, W.; Kollman, P. A. Computational study of protein specificity: the molecular basis of HIV-1 protease drug resistance. *Proc. Natl. Acad. Sci. U.S.A.* **2001**, *98*, 14937–14942.

(38) Jarmula, A.; Fraczyk, T.; Cieplak, P.; Rode, W. Mechanism of influence of phosphorylation on serine 124 on a decrease of catalytic activity of human thymidylate synthase. *Bioorg. Med. Chem.* **2010**, *18*, 3361–3370.

(39) Zhang, J.; Li, C.; Shi, T.; Chen, K.; Shen, X.; Jiang, H. Lys169 of human glucokinase is a determinant for glucose phosphorylation: implication for the atomic mechanism of glucokinase catalysis. *PLoS One* **2009**, *4*, e6304.

(40) Rocchia, W.; Alexov, E.; Honig, B. Extending the applicability of the nonlinear Poisson-Boltzmann equation: multiple dielectric constants and multivalent ions. *J. Phys. Chem. B* **2001**, *105*, 6507–6514.

(41) Fiol, C. J.; Mahrenholz, A. M.; Wang, Y.; Roeske, R. W.; Roach, P. J. Formation of protein kinas recognition sites by covalent modification of the substrate. *J. Biol. Chem.* **1987**, *262*, 14042–14048.

(42) Thomas, G. M.; Frame, S.; Goedert, M.; Nathke, I.; Polakis, P.; Cohen, P. A GSK3-binding peptide from FRAT1 selectively inhibits the GSK3-catalysed phosphorylation of Axin and β-catenin. *FEBS Lett.* **1999**, *458*, 247–251.

(43) Cheng, Y.; Zhang, Y.; McCammon, J. A. How does the cAMP-dependent protein kinase catalyze the phosphorylation reaction: An ab initio QM/MM study. *J. Am. Chem. Soc.* **2005**, *127*, 1553–1562.

(44) De Vivo, M.; Cavalli, A.; Carloni, P.; Recanatini, M. Computational study of the phosphoryl transfer catalyzed by a cyclin-dependent kinase. *Chem.—Eur. J.* **2007**, *13*, 8437–8444.

(45) Zhang, N.; Jiang, Y.; Zou, J.; Yu, Q.; Zhao, W. Structural basis for the complete loss of GSK3β catalytic activity due to R96 mutation investigated by molecular dynamics study. *Proteins* **2009**, *75*, 671–681.

(46) De Vivo, M.; Cavalli, A.; Bottegon, G.; Carloni, P.; Recanatini, M. Role of phosphorylated Thy160 for the activation of the CDK2/Cyclin A/complex. *Proteins* **2006**, *62*, 89–98.

(47) Cox, S.; Taylor, S. S. Kinetic analysis of cAMP-dependent protein kinase: mutations at histidine 87 affect peptide binding and pH dependence. *Biochemistry* **1995**, *34*, 16203–16209.

(48) Alzate-Morales, J. H.; Vergara-Jaque, A.; Caballero, J. Computational study on the interaction of N1 substituted pyrazole derivatives with Raf kinase: An unusual water wire hydrogen-bond network and novel interactions at the entrance of the active site. *J. Chem. Inf. Model.* **2010**, *50*, 1101–1112.

(49) Bártová, I.; Otyepka, M.; Kříž, Z.; Kočá, J. The mechanism of inhibition of the cylinc-dependent kinase-2 as revealed by the molecular dynamics study on the complex CDK2 with the peptide substrate HHASPPK. *Protein Sci.* **2005**, *14*, 445–451.

(50) Díaz, N.; Field, M. J. Insights into the phosphoryl-transfer mechanism of cAMP-dependent protein kinase from quantum chemical calculations and molecular dynamics simulations. *J. Am. Chem. Soc.* **2004**, *126*, 529–542.

(51) Ng, Y.-W.; Raghunathan, D.; Chan, P. M.; Baskaran, Y.; Smith, D. J.; Lee, C.-H.; Verma, C.; Manser, E. Why an A-loop phosphormimetic fails to activate PAK1: Understanding an inaccessible kinase state by molecular dynamics simulations. *Structure* **2010**, *18*, 879–890.